Modeling of multiple-scattering suppression by a one-beam cross-correlation system

Vladimir I. Ovod

I detail the results of adapting a rigorous algorithm, derived for multiple-scattering simulations in photon correlation spectroscopy, for modeling multiple-scattering suppression by a cross-correlation system that employs one laser beam and two slightly tilted detectors. The practical significance of the proposed numerical technique is shown for optimization of an arbitrary design configuration of cross correlation and for prediction of the ideal performance that is possible with that design. It is shown that the behavior of the coherent factor modeled versus the angle between detectors is in agreement with experimental data and analytical investigation. This factor permits mapping of the spatial extent of the single-scattering and the multiple-scattering speckles. The map holds important information about the optimal displacement of detectors for a given measurement setup, and it permits a comprehensive investigation of suppression of the scattering components, even when their magnitudes are small.

OCIS codes: 120.5820, 290.4210, 290.5850, 290.7050.

1. Introduction

Numerical modeling of multiple scattering by dispersed systems, which affects particle characterization in photon correlation spectroscopy, is of key importance for improving the spectroscopy's performance parameters.[1,2] The commonly used methods for multiple-scattering simulation in semidilute systems[3–5] and in dense suspensions[6,7] are monomer-based methods. In other words, they do not permit the simulation of the scattering cross section of an ensemble of particles that is characterized by different optical properties and diameters; i.e., they take into account the phase factors of monomers and the scattering cross section of single particles only. Diffusing wave spectroscopy[6] and correlation transfer theory[7] are built on knowledge of the single-scattering correlation function, which is often unknown.

To overcome the limitations mentioned above, Ovod *et al.*[8] recently derived and introduced a new technique for the investigation of fine multiple-scattering effects in fiber optic photon correlation spectroscopy. The technique involves the algorithm developed by Mackowski[9,10] for use of a rigorous calculation of the scattering of a plane wave from multiple-sphere clusters instead of the Rayleigh–Gans–Debye approximation.[3–5] One of the best advantages of using the rigorous multiple-scattering technique instead of the Rayleigh–Gans–Debye approximation in the important range of 0.05–5-μm particle diameters is the following: This rigorous technique allows for the estimation of the performance characteristics of different particle sizers (based on the dynamic as well on the static light-scattering phenomena) in the broad range of particles' refractive indices.

In this paper I detail the results of adapting the rigorous algorithm for the simulation of multiple-scattering suppression in the far zone by a new one-beam cross-correlation system. The new cross-correlation method for characterizing particles in turbid media was studied experimentally[11,12] and analytically.[13] The method relies on the positioning of two detectors on the same single-scattering coherence area but on different multiple-scattering coherence areas, which are physically smaller than the single-scattering speckle.

It is my aim in this paper to provide a comprehensive analysis of the multiple-scattering suppression phenomena in cross-correlation by numerical modeling and to demonstrate the perspectives of the pro-

When this research was performed, the author was with Particle Sizing Systems, 75 Aero Camino, Santa Barbara, California 93117 and the Department of Chemistry, University of California at Santa Barbara, Santa Barbara, California 93106. He can be reached by email at vovod@hotmail.com.

Received 14 November 1997; revised manuscript received 7 August 1998.

0003-6935/98/337856-09$15.00/0

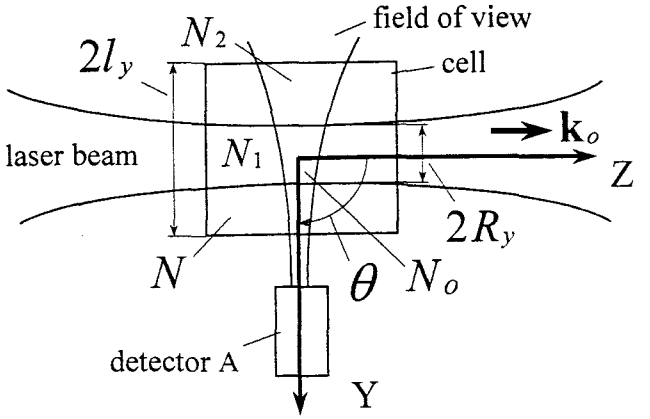

Fig. 1. Schematic representation of the cross-correlation setup at $\theta = 90°$. Hidden detector B is located in the same x–y plane as is shown for the detector A. A laser beam propagates through a scattering cell of volume V, illuminating sample volume V_1. Both detectors view the same sample volume, V_2. The intersection of V_1 and V_2 volumes is denoted V_o. The average numbers of particles in these volumes are N, N_1, N_2, and N_o, respectively.

posed numerical technique for the optimization of an arbitrary design configuration of cross correlation and prediction of the ideal performance that is possible with that design. It is shown that the behavior of the coherent factor modeled versus the angle between detectors is in agreement with experimental data[12] and analytical investigation.[13] This factor permits mapping of the spatial extent of the single-scattering and multiple-scattering speckles. The map holds important information about the optimal displacement of detectors for a given measurement setup, and it permits a comprehensive investigation of the suppression of the scattering components even if their magnitudes are small. As an example, the quantitative estimation of the negligence of the contribution of the perpendicular single-scattering component to the cross-correlation function, which was first shown experimentally,[12] is provided here by numerical modeling.

The body of this paper is organized as follows. In Section 2 the cross-correlation setup is described. The algorithm for the rigorous simulation of single- and multiple-order scattering by an ensemble of moving particles is discussed in Section 3. The scheme used for the calculation of the intensity cross-correlation function is described briefly in Section 4. In Section 5 the contribution of the second-order scattering to the intensity cross-correlation function from an ensemble of 9000 spheres is calculated. It is shown that this technique permits setup optimization even if the amount of multiple scattering is small.

2. Cross-Correlation Setup

The scattering geometry is shown in Fig. 1. A laser beam of wavelength λ in vacuum and angular frequency ω propagates along the z axis of the XYZ experimental coordinate system. A particle suspension of volume fraction $\phi = \pi d^3 \rho_v/6$ in a cell of volume $V = 2l_x 2l_y 2l_z$ scatters light into point detectors A and B in the far field. The detectors' locations are given by the spherical coordinates $\{\theta_A = \theta, \varphi_A = \varphi - \delta\}$ and $\{\theta_B = \theta, \varphi_B = \varphi_B = \varphi + \delta\}$, respectively, with $\theta = 90°$ and $\varphi = 90°$. In other words, both detectors are located in the xy plane. The average number density of the particles suspended in a nonabsorbing liquid of real refractive index n_L is defined by $\rho_v = N/V$, where N is the number of monodispersed spheres of diameter d_p and refractive index $m_p = n_p + i\chi_p$. Both detectors view the same sample volume, V_2, and the laser illuminates sample volume V_1. The intersection of these two volumes, denoted by V_o, is a source of single scattering by particles. The average numbers of particles in these volumes are N_2, N_1, and N_o.

As is shown first,[13] considering the volume V_o to be a cylinder of radius R_x and length $2R_z$ the spatial coherence area of the single scattering far down the y axis can be estimated by the angular diameters

$$\delta_{\mathrm{coh}}^{x} = \frac{1}{kR_x}, \tag{1}$$

$$\delta_{\mathrm{coh}}^{z} = \frac{1}{kR_z} \tag{2}$$

in the x and z directions, respectively, where

$$k \equiv |\mathbf{k}_o| = \frac{2\pi n_L}{\lambda} \tag{3}$$

is the wave number of the light in the liquid and $\mathbf{k}_o$ is the wave vector of the incident field. To map out the spatial extent of the single-scattering and the multiple-scattering speckles, we use a rigorous algorithm for multiple-order scattering simulation.

3. Multiple-Order Scattering By an Ensemble of Moving Spheres

A. Scattering by an Isolated Spherical Particle

In the context of rigorous Mie theory,[14] the electric field, $\mathbf{E}_{s,\varepsilon}^{i}$, scattered by an isolated spherical particle i, that satisfies Maxwell's wave equations can be expressed in terms of an infinite series of the vector spherical functions $\mathbf{M}$ and $\mathbf{N}$ (with the origin of coordinates at the center of particle i) as

$$\mathbf{E}_{s,\varepsilon}^{i} = E_o^i D(\mathbf{X}^i) \sum_{n=1}^{\infty} \sum_{m=-n}^{n} [a_{mn1,\varepsilon}^{i} \mathbf{N}_{mn}^{(3)}(k\mathbf{R}_d^i) + a_{mn2,\varepsilon}^{i} \mathbf{M}_{mn}^{(3)}(k\mathbf{R}_d^i)], \tag{4}$$

where $\mathbf{X}^i$ is the position vector of the origin of particle i in the XYZ experimental coordinate system, $\mathbf{R}_d^i$ is the vector between the origin of particle i and a point detector d, $D(\mathbf{X}^i)$ is the relative sensitivity of detector d,[12,13] and $a_{mn\,p,\varepsilon}$ are the scattered field expansions (or so-called partial-wave scattering amplitudes) of order n and degree m. The extra index p denotes the mode, in which $p = 1$ and $p = 2$ refer to the TM and the TE modes, respectively, of the scattered field.

The subscript ε denotes X ($\varepsilon = X$) or Y ($\varepsilon = Y$) polarization of the incident beam. As we are working in the framework of elastic light scattering, we omit the time-dependent term $\exp(-i\omega t)$ from all formulas, as is the normal practice. The incident field strength in the z^i cross section is given by

$$E_o^i = E_o \exp(ikL_e)\exp\left(-k_m^{im}\frac{L_{bi}}{2}\right), \tag{5}$$

were E_o is the field strength of the incident beam, L_e is the distance that the beam has traveled to the origin e of the experimental coordinate system, and L_{bi} is the distance that the beam has traveled through the suspension of turbidity k_m^{im} (in fact, k_m^{im} is the imaginary part of the wave number of light in a dispersed system) to the origin of particle i. The vector of the scattered field $\mathbf{E}_{s,\varepsilon}^i$, the vector spherical harmonics $\mathbf{M}_{mn}$ and $\mathbf{N}_{mn}$, and the vector $\mathbf{R}_d^i$ are given in a spherical coordinate system (R^i, θ^i, and φ^i) of sphere i. The superscript (3) on the coefficients denotes that the coefficients are based on the spherical Hankel functions. The scattering problem (as well as the problem of internal field) from a single sphere is solved exactly[14]; i.e., the partial-wave scattering amplitudes are expressed in terms of the incident plane wave as

$$a_{\pm 1np,\varepsilon}^{i,s=1} = -\alpha_{np}^i U(\mathbf{X}^i) p_{\pm 1np,\varepsilon} \exp(i\mathbf{k}_o\mathbf{X}^i), \tag{6}$$

where α_{n1} and α_{n2} are the well-known TM and TE Lorenz–Mie coefficients of the isolated sphere i,[10,14] $U(\mathbf{X})$ is a dimensionless function that describes the transverse beam profile,[13] the superscript $s = 1$ denotes that only single scattering is taken into account, and, as usual, $\mathrm{i} = (-1)^{1/2}$ is the unit imaginary number. The expansion coefficients of the incident plane wave propagating in direction z are given by[9]

$$p_{1n1,x} = \frac{-\mathrm{i}^{n+1}}{2}\frac{2n+1}{n(n+1)}, \tag{7}$$

$$p_{-1n1,x} = \frac{\mathrm{i}^{n+1}}{2}(2n+1),$$

$$p_{mnp,\varepsilon} = 0, \qquad |m| \neq 1,$$

$$p_{mn(3-p),\varepsilon} = m p_{mnp,\varepsilon}, \qquad p_{mnp,y} = \frac{1}{\mathrm{i}} p_{mn(3-p),x}. \tag{8}$$

B. Scattering by an Ensemble of Spherical Particles

When an ensemble of N particles is illuminated by a plane wave, i.e., $N_3 = N$, the field incident upon sphere i comprises the field scattered by j sphere, which is written in the j coordinate system. To solve the scattering problem by sphere i, we must now express the field scattered by sphere j in the coordinate system of sphere i. This is accomplished by use of the translation addition theorem for spherical wave functions.[9,10] By using this theorem we can find the amount of the additional (multiple, $s = 2$) scattering from sphere i (caused by the above-mentioned contribution of spheres $j \neq i$) by

$$a_{mnp,\varepsilon}^{i,s=2} = -\alpha_{np,\varepsilon}^i \sum_{\substack{j=1 \\ j\neq i}}^{N_3} \sum_{l=1}^{N_o^j} \sum_{k=-l}^{l} [A_{klmn}^{(3)}(kR^{ij}, \Theta^{ij}, \Phi^{ij}) a_{mnp,\varepsilon}^j + B_{klmn}^{(3)}(kR^{ij}, \Theta^{ij}, \Phi^{ij}) a_{mn(3-p),\varepsilon}^j], \tag{9}$$

where the additional coefficients A and B depend entirely on the distance R^{ij} and the direction of translation Θ^{ij}, Φ^{ij} of origin j to i. The required number of orders, N_o^j, in the expansions for the scattered field from the jth sphere can be estimated from the following criterion[10]:

$$N_o^j \approx \rho^j + 4(\rho^j)^{1/3} + 2, \tag{10}$$

where $\rho^j = kd_p^j/2$ is the Mie parameter. The total fields, which are scattered by spheres i and j and incorporate both the single-scattering ($s = 1$) and the multiple-scattering ($s = 2$) components, can now be written, respectively, as

$$a_{mnp,\varepsilon}^i = \sum_{s=1}^{2} a_{mnp,\varepsilon}^{i,s}, \tag{11}$$

$$a_{mnp,\varepsilon}^j = \sum_{s=1}^{2} a_{mnp,\varepsilon}^{j,s}, \tag{12}$$

where

$$a_{\pm 1np,\varepsilon}^{j,s=1} = -\alpha_{np}^j U(\mathbf{X}^j) p_{\pm 1np,\varepsilon} \exp(i\mathbf{k}_o\mathbf{X}^j), \tag{13}$$

$$a_{mnp,\varepsilon}^{j,s=2} = -\alpha_{np,\varepsilon}^j \sum_{\substack{i=1 \\ i\neq j}}^{N_3} \sum_{l=1}^{N_o^i} \sum_{k=-l}^{l} \times [A_{klmn}^{(3)}(kR^{ji}, \Theta^{ji}, \Phi^{ji}) a_{mnp,\varepsilon}^i + B_{klmn}^{(3)}(kR^{ji}, \Theta^{ji}, \Phi^{ji}) a_{mn(3-p),\varepsilon}^i] \tag{14}$$

are the single-scattering ($s = 1$) and the multiple-scattering ($s = 2$) components, respectively, of the sphere j.

The scattering equations are now written for all N particles that participate in the scattering, thus producing a set of coupled ($p = 1, 2$) linear equations (11) for the partial-wave scattering amplitudes. If this set of coupled equations is iterated, the various iteration orders correspond to single scattering, double scattering, triple scattering, etc. The set of coupled equations is most commonly solved by iteration methods[9,10,15,16] or by the order-of-scattering technique.[17,18]

Once all partial-wave scattering amplitudes for all N particles are obtained in their own coordinate systems, the accompanying vector spherical harmonics have to be translated from the individual particle origins back to the common (ensemble) origin, which coincides with the origin of the XYZ coordinate system. This last translation (used in our previous investigation[8] in the so-called single–common-origin approach) causes numerical convergence problems that have been discussed comprehensively in Ref. 19.

These problems are eliminated if one is interested in far-zone scattering only. In this case (so-called multiple-origins approach), the last set of translation coefficients has a straightforward analytical form,[19] and now the problem of exact electromagnetic wave scattering is solved. The scattered electric field, $\mathbf{E}_{s,\varepsilon}$, from the entire ensemble of spheres is taken to be the superposition of scattered fields, $\mathbf{E}^i_{s,\varepsilon}$, from N_2 spheres viewed by the detector, i.e.,

$$\mathbf{E}_{s,\varepsilon} = \sum_{i=1}^{N_2} \mathbf{E}^i_{s,\varepsilon}. \tag{15}$$

C. Far-Zone Approach

Of our practical interest is the detection of the scattered field in the far zone, when smallest distance R^i_d for each sphere is larger than the largest distance between the spheres, R^{ij}. For the far-zone assumption, the spherical Hankel functions can be replaced by their asymptotes,[19] and the orthonormal unit vectors $\hat{r}^i$, $\hat{\theta}^i$, and $\hat{\varphi}^i$ for the i sphere coincide with the corresponding orthonormal unit vectors $\hat{r}$, $\hat{\theta}$, and $\hat{\varphi}$, for the entire ensemble. Taking into account the above-mentioned asymptote of the spherical Hankel functions, we can write the vector spherical functions in the far zone[19] as

$$\mathbf{M}^{(3)}_{mn}(k\mathbf{R}^i_d) = (-\mathrm{i})^{n+1} \frac{\exp(\mathrm{i}\mathbf{k}^i_s\mathbf{R}^i_d)}{kR^i_d} \exp\left(-k^{im}_m \frac{L_{id}}{2}\right) \times [\mathrm{i}\tau_{mn2}(\theta^i)\hat{\theta} - \tau_{mn1}(\theta^i)\hat{\varphi}]\exp(im\varphi^i), \tag{16}$$

$$N^{(3)}_{mn}(k\mathbf{R}^i_d) = (-\mathrm{i})^{n} \frac{\exp(\mathrm{i}\mathbf{k}^i_s\mathbf{R}^i_d)}{kR^i_d} \exp\left(-k^{im}_m \frac{L_{id}}{2}\right) \times [\tau_{mn1}(\theta^i)\hat{\theta} + \mathrm{i}\tau_{mn2}(\theta^i)\hat{\varphi}]\exp(im\varphi^i), \tag{17}$$

where

$$\tau_{mn1}(\theta) = \frac{\mathrm{d}}{\mathrm{d}\theta} P^m_n \cos(\theta), \qquad \tau_{mn2}(\theta) = \frac{m}{\sin(\theta)} P^m_n \cos(\theta) \tag{18}$$

are the scattering functions, P^m_n stands for the associated Legendre function of the first kind, and L_{id} is the distance in the suspension from the origin of particle i to point detector d. The scattered wave vector relative to the origin of particle i is defined by

$$\mathbf{k}^i_s = \frac{k\mathbf{R}^i_d}{R^i_d} = k(\sin\theta^i \cos\varphi^i\hat{x} + \sin\theta^i \sin\varphi^i\hat{y} + \cos\theta^i\hat{z}), \tag{19}$$

where $\hat{x}$, $\hat{y}$, and $\hat{z}$ are the unit vectors of the Cartesian coordinate system.

We consider that $R^i_d \approx R_d$ in the far zone and that the relation between the position vectors of sphere i and detector d can be expressed by

$$\mathbf{R}^i_d = \mathbf{R}_d - \mathbf{X}^i. \tag{20}$$

By inserting Eq. (20) into Eqs. (16) and (17), and then Eqs. (16) and (17) into Eq. (4), we obtain

$$\mathbf{E}^i_s = iT\mathbf{P}^i_s, \tag{21}$$

where $\mathbf{R}_d$ is the position vector of the detector in the experimental frame and

$$T = E_o D(\mathbf{X}^i) \frac{\exp(i\mathbf{k}^i_s\mathbf{R}_d)}{kR_d} \exp(ikL_e)\exp\left(-k^{im}_m \frac{L_{bi} + L_{id}}{2}\right) \tag{22}$$

is the coefficient, which does not depend strongly on the motion of particle i. The vector scattering amplitude, $\mathbf{P}^i_s$, reflects the main contribution of the particle motion to the signal in photon cross correlation. The components of vector $\mathbf{P}^i_s$ of the scattering amplitudes, polarized in the $\hat{\theta}$ and $\hat{\varphi}$ directions,[20] are expressed by

$$P^i_\theta = \exp(-\mathrm{i}\mathbf{k}^i_s\mathbf{X}^i)[S^i_2(\theta^i, \varphi^i)e^i_x + S^i_3(\theta^i, \varphi^i)e^i_y], \tag{23}$$

$$P^i_\varphi = \exp(-\mathrm{i}\mathbf{k}^i_s\mathbf{X}^i)[S^i_4(\theta^i, \varphi^i)e^i_x + S^i_1(\theta^i, \varphi^i)e^i_y], \tag{24}$$

where e^i_x and e^i_y are the components of the unit polarization vector of the plane wave that illuminates sphere i and

$$S^i_1(\theta^i, \varphi^i) = \sum_{n=1}^{\infty}\sum_{m=-n}^{n}\sum_{p=1}^{2} (-\mathrm{i})^n a^i_{mnp,\varepsilon=y}\tau_{mn(3-p)}(\theta^i) \times \exp(im\varphi^i), \tag{25}$$

$$S^i_2(\theta^i, \varphi^i) = \sum_{n=1}^{\infty}\sum_{m=-n}^{n}\sum_{p=1}^{2} (-\mathrm{i})^{n+1} a^i_{mnp,\varepsilon=x}\tau_{mnp}(\theta^i) \times \exp(im\varphi^i), \tag{26}$$

$$S^i_3(\theta^i, \varphi^i) = \sum_{n=1}^{\infty}\sum_{m=-n}^{n}\sum_{p=1}^{2} (-\mathrm{i})^{n+1} a^i_{mnp,\varepsilon=y}\tau_{mnp}(\theta^i) \times \exp(im\varphi^i), \tag{27}$$

$$S^i_4(\theta^i, \varphi^i) = \sum_{n=1}^{\infty}\sum_{m=-n}^{n}\sum_{p=1}^{2} (-\mathrm{i})^{n} a^i_{mnp,\varepsilon=x}\tau_{mn(3-p)}(\theta^i) \times \exp(im\varphi^i), \tag{28}$$

are the four elements of the amplitude scattering matrix.[15,20] As was mentioned above, the subscript ε for x or y denotes a scattering coefficient calculated for parallel (along the X axis) or perpendicular (along Y axis) incident polarization, respectively. We assume the same polarization of the incident wave for all particles; i.e.,

$$e^i_x = \frac{E_x}{E_o}, \tag{29}$$

$$e^i_y = \frac{E_y}{E_o}, \tag{30}$$

where E_x and E_y correspond to incident plane-wave polarization in the x and y directions in the cross section of the light emission.

The exponential coefficient in Eqs. (23) and (24) is

the product of Eq. (20) in the above-mentioned multiple-origins scattering approach, and its use eliminates the last translation of the partial-wave scattering amplitudes $a^i_{mnp,\varepsilon}$ in Eqs. (25)–(28) from the origin of each sphere to the common (ensemble) origin. This exponential coefficient confirms that our model is in agreement with published results[19] based on deriving the analytical expression for the vector coefficients of the last translations to the common origin. The computational efficiency of the multiple-origins approximation of the scattering by a particle ensemble in the far zone was investigated recently[19] in comparison with the single-origin approximation for the far-field scattering.[9]

An additional increase in the computational efficiency could be reached by simulation of the second-order scattering only, which is the normal practice in photon correlation spectroscopy.[3–5,13] Second-order scattering obviates the solution of linear equations, and it decreases the upper range of the sum in Eq. (9) by the number of spheres that are being illuminated only, i.e., $N_3 = N_1$. In this case the scattering expansions are simulated by Eq. (11) directly, because the first-order scattering expansions $a^{j1}_{mnp,\varepsilon}$ [Eq. (13)] instead of multiple-order scattering coefficients $a^j_{mnp,\varepsilon}$ [(12)] are taken into account for spheres j. In the second-order approach, Eq. (9) must be modified by

$$a^{i,s=2}_{mnp,\varepsilon} = -\alpha^i_{np,\varepsilon} \sum_{\substack{j=1 \\ j\neq i}}^{N_1} F \sum_{l=1}^{N^j_o} \sum_{k=-l}^{l} [A^{(3)}_{klmn}(kR^{ij}, \Theta^{ij}, \Phi^{ij}) a^j_{mnp,\varepsilon} + B^{(3)}_{klmn}(kR^{ij}, \Theta^{ij}, \Phi^{ij}) a^j_{mn(3-p),\varepsilon}], \quad (31)$$

where the coefficient F reflects the extinction of the scattered light on the path between spheres j and i, which is caused by the ignored higher-order scattering. As in Refs. 3–5 and 13, the coefficient F is defined by

$$F = \begin{cases} 1 & \text{multiple-order scattering} \\ \exp\left(-k^{im}_m \dfrac{R^{ij}}{2}\right) & \text{second-order scattering} \end{cases}. \quad (32)$$

4. Intensity Cross-Correlation Function

The intensity cross-correlation function is defined by[13]

$$G^{(2)}(\tau, \delta) = \int_{-\infty}^{\infty} I_A(t) I_B(t + \tau) \mathrm{d}t, \quad (33)$$

where I_A and I_B denote the time-dependent intensities, which are scattered by measured particles in the fields of view of detectors A and B, respectively, t is the time, and τ means cross-correlation delay time. For the most practical cases when the hydrodynamic interaction of particles does not sufficiently affect the Gaussian stochastics of the scattered electric fields $\mathbf{E}_A$ and $\mathbf{E}_B$, one can use Wick's theorem[3] to model the intensity cross-correlation function by the electric-field terms; i.e.,

$$G^{(2)}(\tau, \delta) = \mathrm{BL} + |Y|^2 + |W|^2, \quad (34)$$

where

$$Y = \int_{-\infty}^{\infty} \mathbf{E}_A(t) \mathbf{E}_B(t + \tau) \mathrm{d}t, \quad (35)$$

$$W = \int_{-\infty}^{\infty} \mathbf{E}^*_A(t) \mathbf{E}_B(t + \tau) \mathrm{d}t;$$

$$\mathrm{BL} = \int_{-\infty}^{\infty} \mathbf{E}^*_A(t) \mathbf{E}_A(t) \mathrm{d}t \int_{-\infty}^{\infty} \mathbf{E}^*_B(t) \mathbf{E}_B(t) \mathrm{d}t \quad (36)$$

is the baseline.

In practice one always measures the normalized intensity cross-correlation function $g^{(2)}(\tau, \delta)$, which can be modeled by

$$g^{(2)}(\tau, \delta) = \frac{G^{(2)}(\tau, \delta) - \mathrm{BL}}{\mathrm{BL}} = \gamma^2(\delta) |g^{(1)}(\tau)|^2, \quad (37)$$

where γ^2 is the coherence factor, or so-called intercept,[12] and $g^{(1)}(\tau)$ is the electric-field cross-correlation function. We never ignore the term Y, even if it is negligible with respect to the term W in our simulations.

For the purpose of investigating the contribution of the single-scattering and multiple-scattering effects to the intensity cross-correlation function separately, the terms Y and W can be expressed by the additional cross terms Y_{fg} and W_{fg},[13] as follows:

$$Y(\tau, \delta) = \sum_{f=1}^{2} \sum_{g=1}^{2} Y_{fg}(\tau, \delta), \qquad W(\tau, \delta) = \sum_{f=1}^{2} \sum_{g=1}^{2} W_{fg}(\tau, \delta), \quad (38)$$

where

$$Y_{fg}(\tau, \delta) = \int_{-\infty}^{\infty} \mathbf{E}_{Af}(t, \delta) \mathbf{E}_{Bg}(t + \tau, \delta) \mathrm{d}t, \quad (39)$$

$$W(\tau, \delta) = \int_{-\infty}^{\infty} \mathbf{E}^*_{Af}(t, \delta) \mathbf{E}_{Bg}(t + \tau, \delta) \mathrm{d}t. \quad (40)$$

The subscripts f and g transmit the corresponding indices 1 and 2 to the superscript s in Eqs. (11)–(14) and (31). Equations (38) are valid when the single-order scattering and the multiple-order scattering are statistically independent. It was shown[3] that this independence is due to the assumption that one must make to use Eq. (38), i.e., that $N_o^2/N_1N_2 \ll 1$. Hence the corresponding fg cross term of the normalized intensity cross-correlation function can be modeled by

$$g^{(2)}_{fg}(\tau, \delta) = \frac{|Y_{fg}(\tau, \delta)|^2 + |W_{fg}(\tau, \delta)|^2}{\mathrm{BL}}, \quad (41)$$

where the term denoted by $fg = 11$ means the single-scattering cross term, $fg = 22$ is the multiple-scattering cross term, $fg = 12$ is the single–multiple cross term, and $fg = 21$ means the multiple–single cross term.

Mapping of the spatial extent of single-scattering ($fg = 11$) speckle, multiple-scattering speckle ($fg = 22$), and the speckles of combined scattering effects (the subscripts f and g are absent in this case) can be performed by the corresponding suppression coefficient

$$C^2_{fg,\mathrm{pol},\varepsilon}(\delta) = \frac{\gamma^2_{fg,\mathrm{pol},\varepsilon}(\delta)}{\gamma^2_{fg,\mathrm{pol},\varepsilon}(\delta = 0)}, \tag{42}$$

where the coherence factor of the fg term (or the contrast[5]) can be written as

$$\gamma^2_{fg,\mathrm{pol},\varepsilon}(\delta) = g^{(2)}_{fg,\mathrm{pol},\varepsilon}(\tau = 0, \delta). \tag{43}$$

The subscript pol for θ or φ shows what kind of component, P_θ or P_φ [Eqs. (23) and (24)], of the vector of the scattering amplitudes $\mathbf{P}_s$ transmits through the polarizer positioned in the front of the detectors. The subscript pol is absent if a polarizer is not used. As in Section 3, the subscript ε for x or y denotes x or y polarization of the incident field.

For optimization purposes and for analysis of the fine effects of multiple scattering when the amount of scattering is small, the relative suppression coefficient can be useful:

$$\mathrm{RC}^2_{fg,\mathrm{pol},\varepsilon}(\delta) = \frac{C^2_{fg,\mathrm{pol},\varepsilon}(\delta)}{C^2_{\mathrm{base}}(\delta)}, \tag{44}$$

where the base coefficient of the relative suppression can be taken arbitrarily, depending on the application. We use the $fg = 11$ and $\varepsilon = x$ subscripts for the base coefficient.

To investigate the scattering components that are negligible at $\delta = 0$ (for example, the θ single-scattering component from an x-polarized incident field, $\gamma^2_{11,\theta,x}$, or the φ single-scattering component from a y-polarized incident field, $\gamma^2_{11,\varphi,y}$), we must define the suppression coefficient for the fg term, $C^2_{fg,\mathrm{pol},\varepsilon}$ [Eq. (42)], taking into account the nonvanished coherence factor, for example $\gamma^2_{\mathrm{pol},\varepsilon}$, to avoid division by zero as

$$C^2_{fg,\mathrm{pol},\varepsilon}(\delta) = \frac{\gamma^2_{fg,\mathrm{pol},\varepsilon}(\delta)}{\gamma^2_{\mathrm{pol},\varepsilon}(\delta = 0)}. \tag{45}$$

The amount of multiple scattering can be estimated by the multiple-to-single scattering ratio as

$$(M{:}S)_{\mathrm{pol},\varepsilon} = \left(\frac{\mathrm{BL}_{22,\mathrm{pol},\varepsilon}}{\mathrm{BL}_{11,\mathrm{pol},\varepsilon}}\right)^{1/2}. \tag{46}$$

5. Computer Simulations and Discussions

As was mentioned above, the aim of our calculations is to provide mapping and analysis of the multiple-scattering suppression phenomena by numerical modeling. When the modeling is performed with a personal computer, the total number of spheres in the investigated suspension is limited to $N = 9000$. These monodispersed spherical particles of diameter $d_p = 0.115$ μm and refractive index $m_p = 1.59 + i0$ are suspended in water of refractive index $n_L = 1.33$. The investigated suspension of volume fraction $\phi = 0.005$ fills the cell of volume V:

$$V = 2l_x 2l_y 2l_z = d_p^3 \frac{\pi N_p}{6\phi}. \tag{47}$$

Below is the estimation of the main parameters (i.e., l_x, l_z, l_y, R_x, R_y, and R_z) of the scattering scheme presented in Fig. 2, which can be used for the demonstration of an effective suppression of the multiple-scattering term.

According to the analytical investigation,[13] the suppression of the multiple-scattering term in the field cross-correlation function can be estimated at the expected detector-displacement angle of $\delta = \delta^x_{\mathrm{coh}}/4$ by

$$C_{22,\varphi,x}\left(\frac{\delta^x_{\mathrm{coh}}}{4}\right) \approx \frac{16\pi R_x}{15\langle R^{ij}\rangle}, \tag{48}$$

where the angle δ^x_{coh} [Eq. (1)] defines the coherence area of the single scattering in the x direction and $\langle R^{ij}\rangle$ means the average displacement between spheres i and j. Hence, if we expect to demonstrate effective suppression of the intensity multiple-scattering term by the coefficient $C^2_{22,\varphi,x} \approx 0.01$, the high of the illuminated volume V_o should be defined by

$$2R_x \approx \frac{15}{8\pi} C_{22,\varphi,x}\left(\frac{\delta^x_{\mathrm{coh}}}{4}\right)\langle R^{ij}\rangle \approx 0.06\langle R^{ij}\rangle. \tag{49}$$

If $2R_x \ll \langle R^{ij}\rangle$ as in relation (49), $l_x = l_z$, and $R_z = R_y = R_x$, then the average displacement $\langle R^{ij}\rangle$ is comparable with $l_z/2$ in the Z direction and with $l_x/2$ in the X direction. Inserting $l_z/2$ instead of $\langle R^{ij}\rangle$ into Eq. (49), we can rewrite Eq. (49) as

$$2R_x \approx 0.06(l_z/2). \tag{50}$$

Now we can show that the set of parameters of the scattering scheme ($2l_x = 2l_z = 45.8$ μm and $2l_y = 2R_x = 2R_y = 2R_z = 0.683$ μm) satisfies Eqs. (47) and (50), and it can be used for illustration of the effective suppression of multiple scattering by the chosen 9000 particles in suspension of volume faction $\phi = 0.005$.

To simplify the modeling we omit the turbidity of the sample, i.e., $k^{im}_m \to 0$, and we assume uniformity of the illuminating field and the fields of view of detectors, i.e., $D = 1$ and $B = 1$. The fields of view of both point detectors are wide enough to permit us to view all 9000 particles contained in the cell. Hence the number of particles in the corresponding volumes of the cell are $N_o = 3$, $N_1 = 3$, and $N_2 = 9000$. For each particle i and for each displacement δ of point detectors A and B located in the far field, we assume two scattered wave vectors characterized in spherical coordinates by $\{R^i_A \approx R_A, \theta^i_A \approx \theta_A = 90°, \varphi^i_A \approx \varphi_A =$

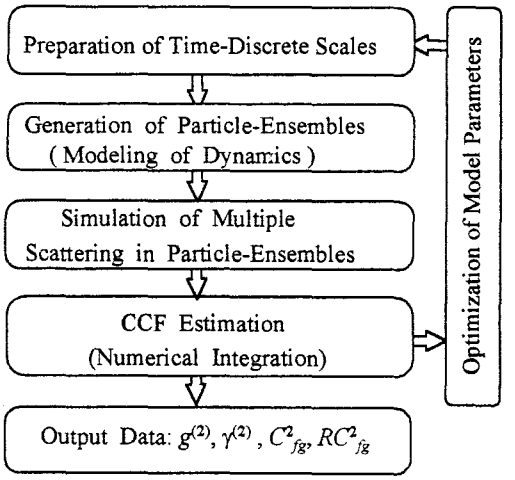

Fig. 2. Flow diagram of the simulations: CCF, cross-correlation function.

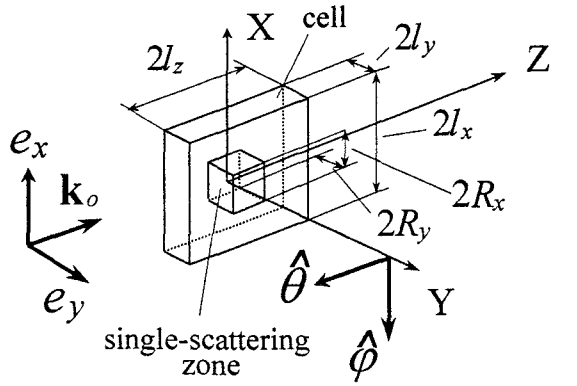

Fig. 3. Scattering schematic illustrating by numerical modeling the multiple-scattering suppression in a particle suspension of volume fraction $\phi = 0.005$. Only volume V_o ($2R_x = 2R_y = 2R_z = 0.683$ μm) contributes to single scattering. The incident field is polarized in the x direction [$e_x = 1$ and $e_y = 0$; Eqs. (23) and (24)] or in the y direction ($e_x = 0$, $e_y = 1$). The orthonormal vectors, $\hat{\theta}$ and $\hat{\varphi}$, denote two polarization states of a receiver polarizer. Two photodetectors view all $N = 9000$ particles contained in the cell of volume V ($2l_x = 2l_z = 45.8$ μm and $2l_y = 0.683$ μm).

$90° - \delta\}$ and $\{R^i_B \approx R_B, \theta^i_B \approx \theta_B = 90°, \varphi^i_B \approx \varphi_B = 90° + \delta\}$, respectively. The wavelength of the illuminated field in vacuum is taken as $\lambda = 0.6328$ μm.

A flow diagram of the modeling is presented in Fig. 2. To model particle dynamics we generate 256 ensembles of 9000 particles in volume V on a discrete scale of time t. The second-order electric field, scattered from 9000 particles, is calculated by Eqs. (15) and (21) and stored for each ensemble. These storage data are used for numerical integration by Eqs. (35), (36), (39), and (40). Details of the particle-dynamic modeling and the numerical integration are not discussed here. These models as well as their optimization, presented schematically in Fig. 2, were published earlier.[8]

Suppression coefficients $C^2_{fg,\mathrm{pol},\varepsilon}(\delta)$ and $C^2_{\mathrm{pol},\varepsilon}(\delta)$, modeled for measurements without any receiver polarizer and with a polarizer transmitting the P_θ component of the scattered light (which is defined in Ref. 12 as a "perpendicular" component for the x-polarized incident field; see Fig. 3), are presented versus the detector displacement in Figs. 4 and Fig. 5, respectively. All results except curve 1 of Fig. 5 were calculated from Eq. (42). Curve 1 of Fig. 5 was obtained from Eq. (45). Two sets of curves (1–3) and (4–6) correspond to the x and y polarizations of the incident field, respectively. Hence curves (1–3) and (4–6) of Fig. 4 correspond to the so-called (VV + VH) and (HV + HH) input–output polarization states, respectively. On the other hand, curves (1–3) and curves (4–6) of Fig. 5 correspond to the VH and HH input–output polarization states, respectively. Here, V denotes vertical polarization of the incident field (input channel) or vertical polarization of the receiver polarizer (output channel) and H means horizontal polarization of the input channel or the output channel (a more detailed definition is given in Ref. 13).

The results show the suppression of the single-scattering cross term C^2_{11} (curves 1 and 4), the second-order scattering cross term C^2_{22} (curves 3 and 6 for $f =$ 2 and $g = 2$), and the modeled cross-correlation function C^2 (curves 2 and 5). The map of the single-scattering coherence area (curve 1 of Fig. 4) is in agreement with analytical estimation [Eq. (1)]. In general, we have reached the goal of these investigations: curve 3 of Fig. 4 illustrates the effectiveness of second-order scattering suppression by the cross-correlation technique. As was mentioned above, the numerical model is limited to 9000 illuminated particles for simulations by a personal computer. Because of this limit, the y dimension of our illuminated

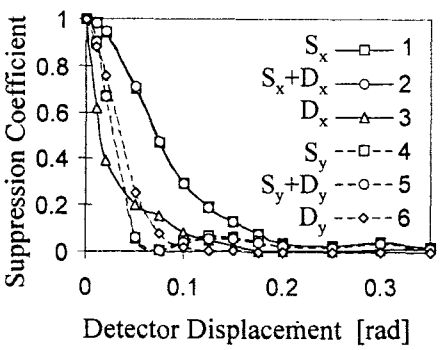

Fig. 4. Suppression of the single-scattering cross term C^2_{11} (curves 1 and 4), the second-order scattering cross term C^2_{22} (curves 3 and 6), and the modeled cross-correlation function C^2 (curves 2 and 5) versus detector displacement. The receiver polarizer is absent. The numbers of particles in the corresponding volumes are $N_o = 3$, $N_1 = 3$, and $N_2 = 9000$. Two sets of curves (curves 1–3 and 4–6) correspond to the x and y polarization, respectively, of the incident field. The detector displacement range of 0.05–0.07 rad can be used as the optimal one for a given scattering geometry. S, D, and $S + D$ denote single, double, and combined (single and double) scattering, respectively. The subscripts x and y correspond to x and y polarization, respectively, of the incident field. Hence curves 1–3 and 4–6 correspond to the so-called (VV + VH) and (HV + HH) input–output polarization states, respectively.

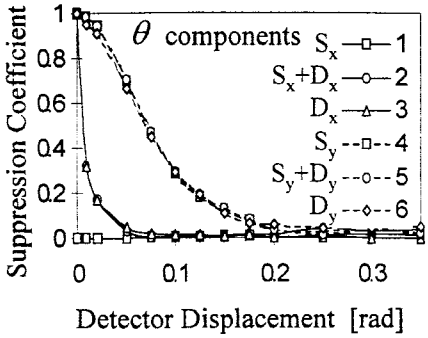

Fig. 5. Suppression of the single-scattering cross term C_{11}^2 (curves 1 and 4), the second-order scattering cross term C_{22}^2 (curves 3 and 6), and the modeled cross-correlation function C^2, (curves 2 and 5) versus detector displacement. Only the P_θ component of the scattered light is transmitted through the detector polarizer. The numbers of particles in the corresponding volumes are $N_o = 3$, $N_1 = 3$, and $N_2 = 9000$. Two sets of curves (curves 1–3 and 4–6) correspond to x and y polarization, respectively, of the incident field. The single-scattering speckle (curve 1) disappears for the x-polarized incident field, as was shown first experimentally.[12] S, D, and S + D denote single, double, and combined (single and double) scattering, respectively. The subscripts x and y correspond to x and y polarization, respectively, of the incident field. Hence curves 1–3 and 4–6 correspond to the VH and HH input–output polarization states, respectively.

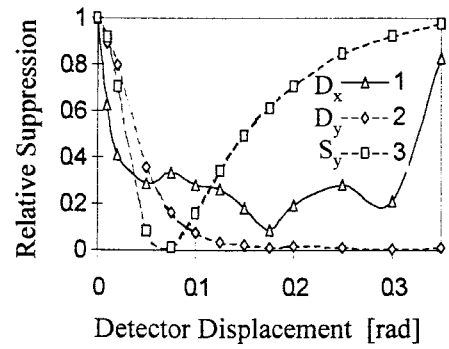

Fig. 6. Relative suppression coefficient $RC^2(\delta)$ versus the detector displacement for three scattering components: the second-order scattering component from the x-polarized incident field (curve 1) and second-order scattering (curve 2) and single-scattering (curve 3) from a y-polarized incident field. The detector displacement range of 0.05–0.07 rad can be used as the optimal one for a given scattering geometry. S and D denote single and double scattering, respectively. The subscripts x and y correspond to x and y polarization, respectively, of the incident field.

volume is limited too. As a result, the average interparticle displacement $\langle R^{ij} \rangle$ in the Y direction is much smaller than in the X and Z directions, and curve 3 illustrates second-order suppression by a value that is larger than the expected suppression C_{22}^2 of 0.01.

Curve 1 and the coincidence of curves 2 and 3 of Fig. 5 give a quantitative estimation of the degree to which the contribution of the perpendicular single-scattering component to the cross-correlation function has been neglected, as was shown first experimentally.[12] As in Ref. 12, the modeling confirms the multiple-to-single scattering ratio, $(M{:}S)_{\theta,x}$, of 1:0 for the perpendicular component. In Fig. 6 the relative suppression coefficient $RC^2(\delta)$ is plotted versus the detector displacement for three scattering components. The coefficient is found relative to the single-scattering component for an x-polarized incident field, $C_{11x}^2(\delta)$. The receiver polarizer is absent. Curve 1 corresponds to the double-scattering component from the x-polarized incident field. Curves 2 and 3 are plotted for second-order scattering and single scattering from a y-polarized incident field. Analysis of Fig. 6 shows that the detector displacement range of 0.05–0.07 rad can be used as the optimal one for a given scattering geometry. Modeling of the square root from the intensity cross-correlation function $g^{(2)}(\tau)$, which is presented in Fig. 7 on a semilogarithmic scale, confirms the phenomenon of multiple-scattering suppression by cross correlation.

The results were found for the single-scattering term, $g_{11}^{(2)}(\tau)$ (curves 2 and 3) and for the second-order scattering cross term $g_{22}^{(2)}(\tau)$ (curves 4 and 5) at δ = 0.05 rad. Curve 1 corresponds to the field autocorrelation function $g^{(1)}(\tau)$ of an ideal system of Brownian particles. Two sets of curves, curves 2 and 4 and 3 and 5, show the contributions of the x and y polarizations, respectively, of the incident field. The symbol τ^* presented first in Fig. 7 denotes the decay time of the cross-correlation function. It is evident that all scattering components were suppressed well at δ = 0.05 rad, except the single-scattering component for an x-polarized incident field (curve 2). The modeling permits the prediction of the nonexponential behavior of multiple-scattering components (curves 4 and 5 in Fig. 7) despite the small multiple-to-single scattering ratio, $M{:}S$, of approximately 1:650 for the given sample. This ratio is in agreement with recently published results.[12]

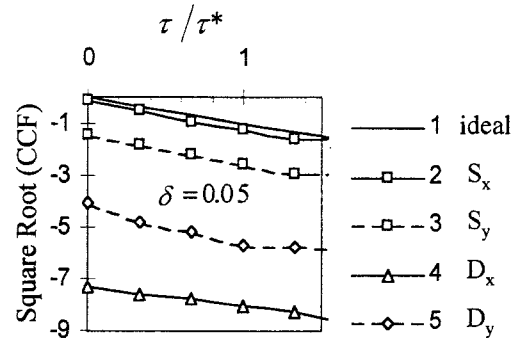

Fig. 7. Square root of the intensity cross-correlation function (CCF) modeled for the single-scattering term, $g_{11}^{(2)}(\tau)$ (curves 2 and 3), and for the second-order scattering cross term, $g_{22}^{(2)}(\tau)$ (curves 4 and 5), and at δ = 0.05 rad and for a system of Brownian particles (curve 1). Curves 2 and 4 are for an x-polarized incident field; curves 3 and 5 are for a y-polarized incident field. S, D, and $S + D$ denote single, double, and combined (single and double) scattering, respectively. The subscripts x and y correspond to x and y polarization, respectively, of the incident field.

6. Conclusions

An effective application has been shown of the proposed numerical model for providing a comprehensive analysis of multiple-scattering suppression by a new cross-correlation technique. In addition to experimental[11,12] and analytical[13] investigations, the modeling confirms that the multiple-scattering speckle is smaller than the single-scattering speckle, which can be estimated by Eq. (1) and examined precisely by mapping of these speckles as shown in Figs. 4 and 6.

These maps hold important information about the optimal displacement of detectors for a given measurement setup with an arbitrary configuration and about the predicted suppression of different scattering components even if their magnitudes are small. As an example, quantitative estimation of the degree to which the contribution of the perpendicular single-scattering component to the cross-correlation function has been neglected, which was shown first experimentally,[12] is presented in Fig. 5. Changing the history of particle dynamics,[8] yields reproducible results.

Modeling of the normalized intensity cross-correlation function permits prediction of the nonexponential behavior of multiple-scattering components (curves 4 and 5 of Fig. 7) despite the small multiple-to-single scattering ratio. Further increasing the computation effectiveness of the proposed technique will permit the modeling and prediction of the performance characteristics of more-realistic arbitrary scattering and illuminating[21] schemes.

The author is grateful to D. W. Mackowski for many useful discussions concerning his code, which he allowed me to adapt for applications in photon correlation spectroscopy. I also thank W. V. Meyer, J. A. Lock, and D. S. Cannell for acquainting me with their results that are relatively analytical and experimental investigations of multiple-scattering suppression. I am grateful to anonymous referees for their valuable comments and suggestions.

References

1. H. Wiese and D. Horn, "Single-mode fibers in fiber-optic quasielastic light scattering: a study of the dynamics of concentrated latex dispersions," J. Chem. Phys. **94,** 6429–6443 (1991).
2. R. G. W. Brown and A. E. Smart, "Practical consideration in photon correlation experiments," Appl. Opt. **36,** 7480–7492 (1997).
3. J. K. G. Dhont and C. G. de Kruif, "Scattered light intensity cross correlation. 1. Theory," J. Chem. Phys. **79,** 1658–1663 (1983).
4. J. K. G. Dhont, "Multiple Rayleigh–Gans–Debye scattering in colloidal systems—dynamic light scattering," Physica A **129,** 374–394 (1985).
5. J. K. G. Dhont and C. G. de Kruif, "Scattered light intensity cross correlation. II. Experimental," J. Chem. Phys. **84,** 45–49 (1986).
6. D. J. Pine, D. A. Weitz, J. X. Zhu, and E. Herbolzheimer, "Diffusing-wave spectroscopy: dynamic light scattering in the multiple scattering limit," J. Phys. (Paris) **51,** 2101–2127 (1990).
7. R. L. Dougherty, B. J. Ackerson, N. M. Reguigui, F. Dorii-Nowkoorani, and U. Nobbmann, "Correlation transfer: development and application," J. Quant. Spectrosc. Radiat. Transfer **52,** 713–727 (1994).
8. V. I. Ovod, D. W. Mackowski, and R. Finsy, "Modeling of the effect of multiple scattering in photon correlation spectroscopy: plane-wave approach," Langmuir **14,** 2610–2618 (1998).
9. D. W. Mackowski, "Analysis of radiative scattering for multiple sphere configuration," Proc. R. Soc. London Ser. A **433,** 599–614 (1991).
10. D. W. Mackowski, "Calculation of total cross sections of multiple-sphere clusters," J. Opt. Soc. Am. A **11,** 2851–2861 (1994).
11. W. V. Meyer, D. S. Cannell, A. E. Smart, T. W. Taylor, and P. Tin, "Multiple scattering suppression by cross correlation," Appl. Opt. **36,** 7551–7558 (1997).
12. U. Nobbmann, S. W. Jones, and B. J. Ackerson, "Multiple scattering suppression: cross correlation with tilted single-mode fibers," Appl. Opt. **36,** 7571–7576 (1997).
13. J. A. Lock, "The role of multiple scattering in cross-correlated light scattering employing a single laser beam," Appl. Opt. **36,** 7559–7570 (1997).
14. H. C. van de Hulst, *Light Scattering by Small Particles* (Dover, New York, 1981).
15. D. W. Mackowski and M. I. Mischenko, "Calculation of the T matrix and scattering matrix for ensembles of spheres," J. Opt. Soc. Am. A **13,** 2266–2278 (1996).
16. Y.-L. Xu, "Electromagnetic scattering by an aggregate of spheres," Appl. Opt. **36,** 4573–4588 (1995).
17. K. A. Fuller and G. W. Kattawar, "Consummate solution to the problem of classical electromagnetic scattering by an ensemble of spheres. 1. Linear chains," Opt. Lett. **13,** 90–92 (1988).
18. K. A. Fuller and G. W. Kattawar, "Consummate solution to the problem of classical electromagnetic scattering by an ensemble of spheres. 1. Clusters of arbitrary configuration," Opt. Lett. **13,** 1063–1065 (1988).
19. Y.-L. Xu, "Electromagnetic scattering by an aggregate of spheres: far field," Appl. Opt. **36,** 9496–9508 (1997).
20. G. Videen, R. G. Pinnick, D. Ngo, Q. Fu, and P. Chýlek, "Asymmetric parameter and aggregate particles," Appl. Opt. **37,** 1104–1109 (1998).
21. V. I. Ovod, "Modeling of multiple scattering from ensemble of spheres in a laser beam," in *Proceedings of the Fifth International Congress on Optical Particle Sizing* (Minneapolis, Minn., 1998).